I
DNA-based Nanomaterials

Nanotechnologies for the Life Sciences Vol. 2
Biological and Pharmaceutical Nanomaterials. Edited by Challa S. S. R. Kumar

ISBN: 3-527-31382-6

1
Self-assembled DNA Nanotubes

Thom LaBean and Sung Ha Park

1.1
Introduction

DNA, well-known as the predominant molecule for the storage of genetic information in biology and biochemistry, has also been recognized as a useful building material in the field of nanotechnology [1–3]. DNA provides basic building blocks for constructing functionalized nanostructures with four major features: molecular recognition, self-assembly, programmability and predictable nanoscale geometry. The limitations of conventional methods of top-down fabrication make bottom-up self-assembled nanostructures using DNA molecules a fascinating and attractive technique for near-term nano/biotechnologies. Recently, self-assembled DNA nanostructures utilizing branched DNA tiles have been reported on (a) various artificial geometrical structures like one- (1-D) and two-dimensional (2-D) periodically patterned structures [4–14], and three-dimensional (3-D) polyhedra [15, 16], and (b) functionalized lattices such as mechanical devices [17–23], molecular computers [24–30] and scaffolds for organizing other functionalized molecules [31–33]. DNA nanostructures are created via self-assembly during the slow annealing of aqueous solutions of carefully designed single-strand DNA, thereby facilitating hybridization of complementary nucleotide sequences, and the formation of double-strand domains and Holliday junction-like crossover points.

In this chapter, we review recent results on self-assembled 1-D DNA nanotubes with unique design schemes and characteristics. DNA nanotubes are characterized by (a) a high aspect ratio, (b) a long, narrow central channel and (c) DNA sidewalls. The 1-D nanotubes are typically made from rolled-up sheets of DNA lattice containing tiles with a variety of motifs: double-crossover (DX) [34], triple-crossover (TX) [35] and four four-arm junctions (4×4) [36]. Schematic drawings of four distinct DNA tile motifs which have been used for constructing complex 1-D DNA nanotubes are shown in Fig. 1.1.

The DNA tiles shown in Fig. 1.1 have each been shown to form large two-dimensional lattice sheets up to 10 μm on an edge, as well as nanotubes formed by lattices which curl and close upon themselves. Superstructure morphology

Nanotechnologies for the Life Sciences Vol. 2
Biological and Pharmaceutical Nanomaterials. Edited by Challa S. S. R. Kumar

ISBN: 3-527-31382-6

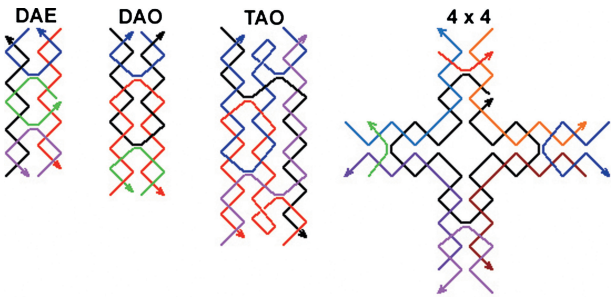

Fig. 1.1. Four distinct DNA motifs for constructing complex 1-D DNA nanotubes. The structures DAE, DAO and TAO are named by acronyms describing their basic characteristics. Names begin with "D" for DX (two helical domains) and "T" for TX (three helical domains). The second character indicates the relative orientations of their two double-helical domains. Here, "A" stands for antiparallel and indicates that, upon crossing over, the strands change direction of propagation along the helical axes. The third character refers to the number of helical half-turns between crossovers, "E" for an even number and "O" for an odd number. The 4 × 4 tile contains four four-arm branched junctions pointing in four directions (north, south, east and west in the tile plane). Arrows indicate simplified strands running from 5′ to 3′.

(sheet versus tube) is controlled in these tiling systems by a variety of means, including counterion concentration, lattice corrugation schemes and disulfide bridge formation. As explained in detail below, curled lattice DNA nanotubes have been observed with either stacked, circular layers of tiles or with spirally wound, chiral configurations. DNA nanotubes have also been intentionally constructed by stacking six-helix bundle (6HB) tiles one on top the other to form tubes with only a single tile per layer and a single double-helix diameter channel through the center [37].

1.2 DNA Nanotubes Self-assembled from DX Tiles

Recently, several varieties of nanotubes constructed from DX tiles have been reported [10–12]. Two distinct types of nanotubes made from DNA DX complexes are DAE-E and DAE-O (where the final letter in the acronym indicates the even/odd parity of helical half-turns between neighboring strand-exchange points within inter-tile joints). DAE-E DX tile nanotubes have diameters between 7 and 20 nm and lengths as long as 50 μm with a persistence length of around 4 μm; they can be programmed to display a variety of patterns. The DAE-O tile lattice can form ribbon structures many micrometers in length and 40–250 nm in width after hybridization.

1.3
DAE-E DX Tile Nanotubes

The construction and characterization of programmable DAE-E nanotubes displaying several tiling schemes as well as the kinetics of their assembly have been studied and reported [10, 11]. DX tiles were first described over 10 years ago [34]. DNA tiles can be thought of as having two parts: (a) a central core of duplex DNA (illustrated by rectangles in Fig. 1.2) and (b) four single-stranded sticky ends which allow it to bind to other tiles (shown protruding from the tile corners). In this first case, the tile core is made up of five oligonucleotides strands that form two double-helical domains held in rigid orientation with parallel axes by a pair of strand-exchange crossover points (Fig. 1.3a). In the study, two different sequence assignments were made to yield two different cores, which the authors called RE and SE [10]. Given an appropriate set of sticky ends, a single core yields a single tile and the unique sequences for sticky end allows the interactions between tiles to be

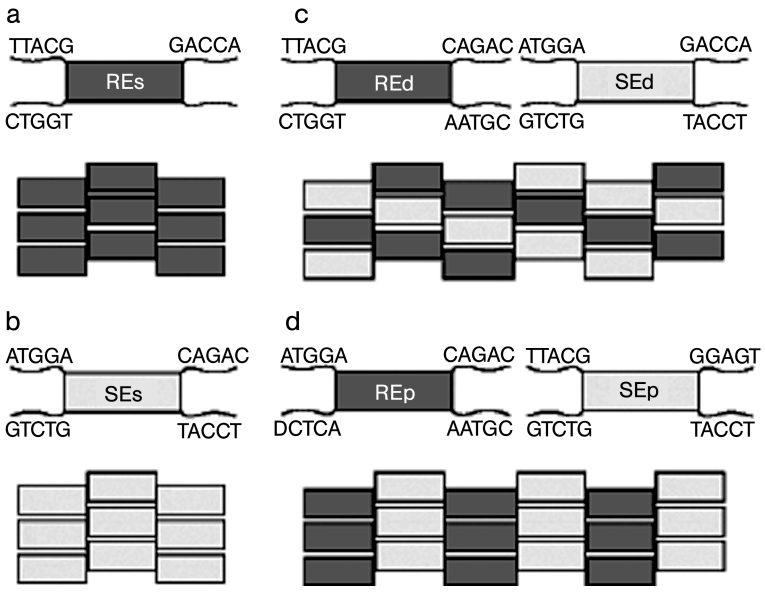

Fig. 1.2. Schematics of lattices utilizing DAE-E tiles. (a) Top: a single REs tile, based on the RE core and carrying four sticky ends. Bottom: complementarity between sticky ends directs the tiles to form a regular lattice. (b) A single SEs tile, based on a different core, SE, and its lattice. (c) Two tiles, REd and SEd, which assemble into a lattice with diagonal stripes; alone each tile could assemble into a linear strip. (d) Another pair of tiles, REp and SEp, cannot assemble independently, but together can form a lattice with stripes perpendicular to the long axis of the tiles. Note: lowercase letters ''s'', ''d'' and ''p'' denote a particular choice of sticky ends and were chosen to represent the pattern generated by the tile set in which they appear: single tile type, diagonally striped or perpendicularly striped lattice. (From Ref. [10].)

programmed (Fig. 1.2). Figure 1.2(c and d) shows how tile sets have been used to create lattices with stripes either diagonal to or perpendicular to the long axis of the tiles. The authors viewed a set of tiles as a program for the construction of a particular structure including a diagonally striped or perpendicularly striped lattice.

In this system, hybridization of complementary sticky end pairs determines whether or not a set of tiles will form a lattice, but the set of sticky ends does not determine whether the lattice will be flat or curved. Curvature is profoundly affected by the choice of lattice symmetry as shown in Fig. 1.3(c–e). The symmetries depicted in Fig. 1.3(c and d) are compatible with flat lattice sheets since deviations

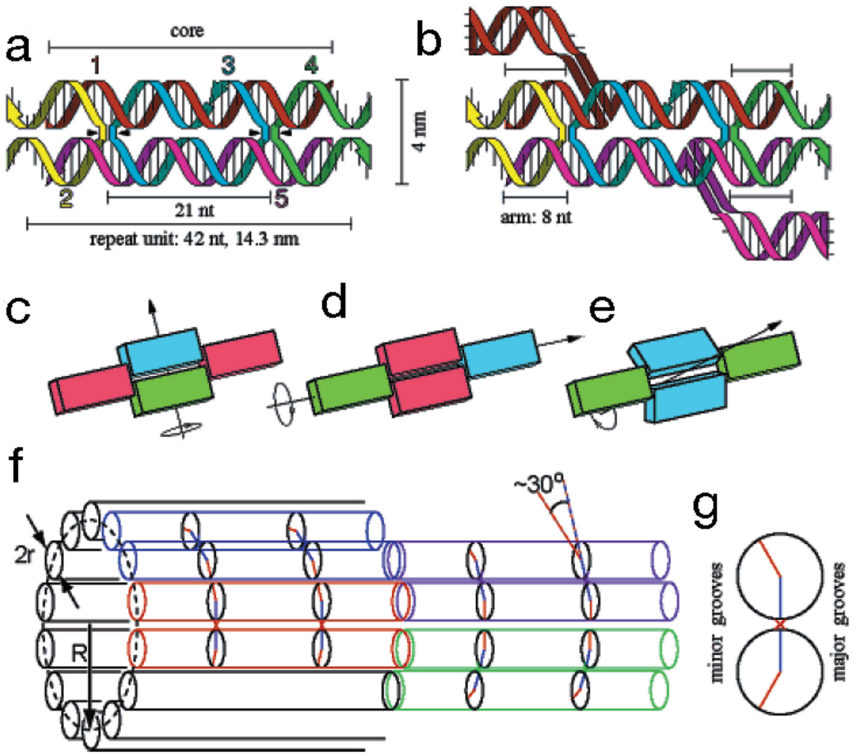

Fig. 1.3. (a) Structure of a DAE-E tile showing numbered strands and their paths through the complex. Tiles contain five single strands with 5-nt sticky ends on strands 2 and 4. (b) Tile structure with hairpins (8-nt stem, 4-nt loop) on strands 1 and 5 between nt 14 and 15 from their 5′-ends. Molecular models suggest that these hairpins attach underneath the molecule, as depicted here; in a tube they would be on the outside. (c and d) Two in-plane rotational symmetries that, if satisfied by a patch of tiles, encourage molecular strain to balance, resulting in a flat sheet. (e) A rotational symmetry, satisfied by DAE-E molecules, that permits curvature. (f) Heptagonal tube of radius *R*. In each tile, two cylinders of radius *r* represent the double helices. Black circles mark crossover points. Blue and orange lines connect the position of phosphate backbones to the center of a helix. The smaller angle between the blue and orange lines defines the minor groove. (g) Cross-section of the red tile from (f) at a crossover point. (From Ref. [10].)

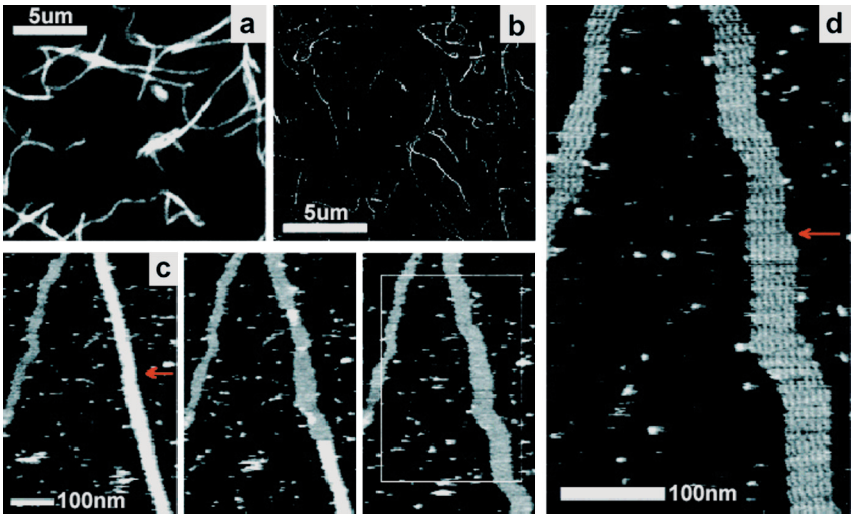

Fig. 1.4. Microscopic images of nanotubes. DNA filaments visualized by (a) fluorescence microscopy and (b) AFM. The solution in (a) contains FAM-labeled REp + SEp and in (b) contains REp + SEp. (c) A time series of AFM images indicates that filaments are tubes (REp + SEp). (Left panel) A thick filament (closed tube) runs the length of the image. Heights of closed tubes suggest they are flattened onto the substrate. An already-open tube is seen on the left. (Center panel) The tube opens progressively from the top, revealing a one-tile-thick lattice. (Right panel) The fully opened tube resembles the lattice on the left. An arrow marks a discrete change in tube width before opening and in the number of tiles after opening, suggesting a defect in the tile lattice. (d) At greater magnification, individual tiles are resolved. (From Ref. [10].)

from planar geometry can be compensated for; thus, molecular strain that could cause curvature may be balanced by symmetric molecular strain elsewhere. Other possible lattice symmetries, such as the one depicted in Fig. 1.3(e), are compatible with intentionally curved lattices and the formation of DNA nanotubes.

DNA nanotubes constructed according to RE- and SE-core tiles were examined by atomic force microscopy (AFM) and by fluorescence microscopy using fluorescein (FAM)-labeled strands. Characterization by AFM showed parallel and diagonal striped patterns, as expected, providing proof that the structural programming functioned properly. AFM studies also revealed that nanotubes flatten out on the mica substrate and were be abraded by the AFM tip from double-layer to single-layer structures by imaging repeatedly at the same place on the sample (Fig. 1.4). The dynamic character of the interactions of nanotubes and lattices with mica was seen by re-imaging a sample by AFM under solution over the course of several hours, and observing tubes coming to and diffusing away from the surface. Fragments of lattice were often left on the mica when a nanotube diffused away. For this reason, the dimensions of the filaments were difficult to measure using surface-based AFM.

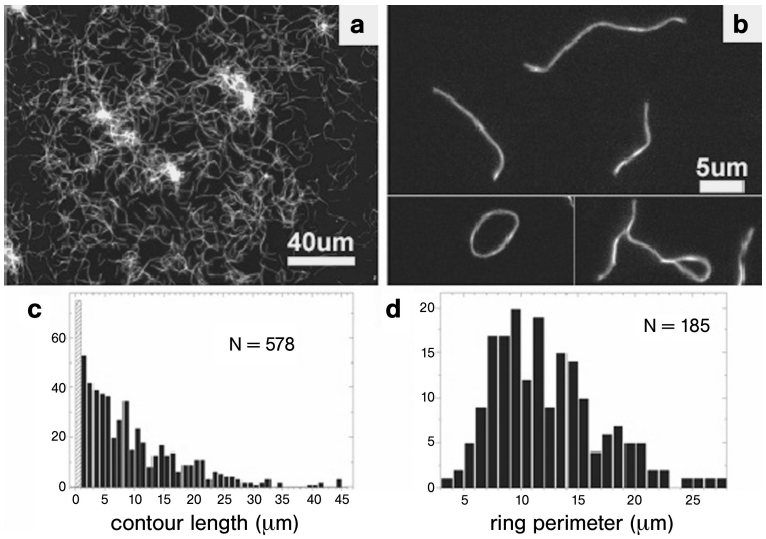

Fig. 1.5. Experimental determination of nanotube persistence length. (a) Epifluorescence image of 400 nM solution of FAM-labeled SEs tubes. Tubes were observed diffusing freely in and out of the focal plane. (b) As (a), but diluted to 40 nM. Occasionally, rings (left) and looped structures (right) are found. (c) Histogram of linear tube lengths with an average of around 7 μm; approximately 10% are over 15 μm long, consistent with an exponential distribution. Some tubes of around 50 μm were observed. (d) Circularized tubes averaged 12 μm in perimeter with a unimodal distribution. The ring shown is typical; most rings are free of kinks that would indicate local weakness. (From Ref. [10].)

Fluorescence microscopy was used to measure the length and stiffness of DAE-E nanotubes in solution. At the highest concentration (400 nM tiles) the density of tubes was too high to identify individuals and clump-like aggregates were common (Fig. 1.5a). Upon 10-fold dilution, single tubes were well dispersed and occasionally a ring or frayed bundle was seen (Fig. 1.5b). Only short tubes were observed directly following annealing and tube lengths continued to increase until about 16 h later when the distribution appeared to stabilize (at which point data were collected; Fig. 1.5c). The mean tube length was around 7 μm with a small proportion of tubes with lengths up to 50 μm being observed.

Tube stiffness was inferred from the distribution of ring perimeters by assuming that the rate of ring formation for a tube of length L is approximately proportional to the fraction of time that the ends of the tube are colocalized at equilibrium. Over brief intervals in which the length distribution does not change significantly, this ring closure probability can be calculated a function of tube length L and persistence length p. Under these conditions, the distribution of ring perimeters should be the product of the distribution of tube lengths and the ring closure probability. The mean perimeter distance was around 12 μm. Using the distributions of Fig. 1.5(c and d), the persistence length was calculated to be 3.85 ± 0.35 μm.

Rothemund *et al.* performed the most thorough examination of the program-

mability and structural properties of DNA nanotubes [10]. They were able to identify the tile faces hidden inside and exposed outside the tubes, and drew important conclusions regarding the placement of hairpins on tiles and their effects on lattice stability. A subset of the authors went on to study the breaking and joining reactions among SEs tile nanotubes and concluded that the growth of DNA tile nanotubes to multimicron length occurs through joining or fusion of preformed nanotubes rather than by sequential addition of individual tiles [11].

1.4
DAE-O DX Tile Nanotubes

A similar system of DNA tiles which was originally designed to form 2-D flat lattice using DAE-O tiles (Fig. 1.6a) was also observed to form nanotubes either with flat ring layers or with spiral layers producing a range of chiral tubes (Figs. 1.6a and 1.7) [12]. As with the study described above, DX tiles (this time of the DAE-O variety) with the four single-stranded sticky ends on each tile were arranged such that α and β tiles tessellate as shown in Fig. 1.6(b). The β tiles contained a 5′-biotinylated strand to enable streptavidin binding to be used as an observable marker. Hybridization was accomplished by cooling the solution by a linear gradient from 96 °C to room temperature over the course of 96 h.

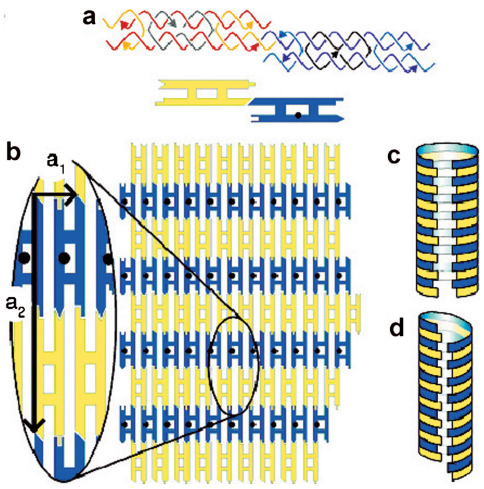

Fig. 1.6. Self-assembly of DAE-O tiles into sheets and tubes. (a) Structure of the DX tiles: colored arrows indicate simplified strands running 5′ to 3′. The 6-nt single-stranded sticky ends on the α tile are complementary to those on the β tile (represented schematically by complementary shapes). A 5′ biotin label on the β tile is shown as a black dot. (b) The α and β tiles can tessellate to form extended 2-D arrays. The 2-D sheets curl and close upon themselves to form tubes, producing either alternating rings (c) or nested helices (d) of α and β tiles. (From Ref. [12].)

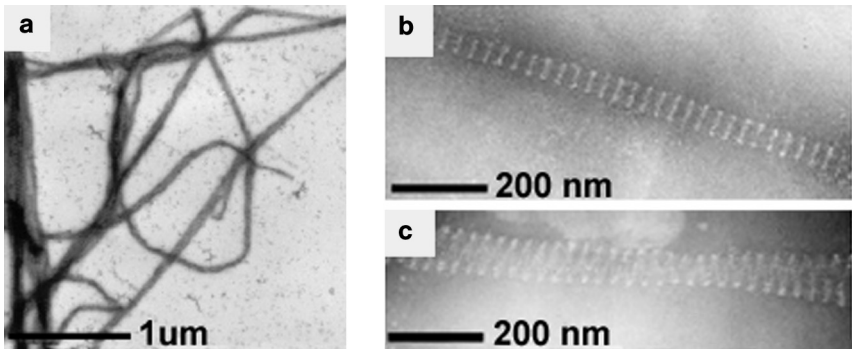

Fig. 1.7. Transmission electron micrographs of negatively stained DNA nanotubules and arrays. White features correspond to points of heavy metal stain exclusion where protein labels are bound to the β tiles. (From Ref. [12].)

In a standard $1 \times \text{TAE/Mg}^{2+}$ buffer, containing 20 mM Tris–acetate, pH 8.3, supplemented with 12.5 mM $MgCl_2$, the tiles form ribbon structures many micrometers in length and 40–250 nm in width after hybridization (Fig. 1.7a). Higher magnification reveals transverse streptavidin bands with a periodicity of 31 ± 2 nm (Fig. 1.7b and c), consistent with the designed 2-D array structure with the long axis of the tiles aligned along the long axis of the ribbons. A natural explanation for the parallel edges of these structures is that arrays of tiles curl and close upon themselves to form tubes. Unambiguous evidence for the formation of tubes is provided by micrographs such as Fig. 1.7(c) in which lines of streptavidin labels zigzag across a ribbon. In all such cases the line is continuous where it changes direction at the edge of the ribbon, proving they represent helical (spiral) tubes with a structure such as that illustrated in Fig. 1.6(d). Mixed superstructure morphologies (tubes and sheets) were observed in buffer with higher salt concentrations.

The authors point out that, as with carbon nanotubes [38], the structure of a DNA nanotube may be characterized by the indices (m, n) of the wrapping vector $\mathbf{c} = m\mathbf{a_1} + n\mathbf{a_2}$ where $\mathbf{a_1}$ and $\mathbf{a_2}$ are basis vectors shown in Fig. 1.6(b), and the tube is formed from a sheet by joining equivalent points separated by $\mathbf{c}$. For nonhelical tubes $n = 0$ (Fig. 1.7b); $n = 1$ where all labels lie on a single helix (Fig. 1.7c). The short dimensions of the tiles are not resolved (the streptavidin labels are larger than the tile width); assuming $\mathbf{a_1} = 4$ nm, then $m \sim 40$ (Fig. 1.7c). It is likely that tube diameters are determined by nonequilibrium processes, since once a tube has closed, an activation barrier prevents further lateral growth. Tube formation reduces the free energy of a tile array by satisfying all inter-tile bonds except those at the ends of the tube. Intrinsic curvature of the array would facilitate tube formation; however, the odd number of helical half-turns along the arms joining crossover points on adjacent tiles means that in this system the intrinsic curvatures of α and β tiles are opposed.

1.5
TX Tile Nanotubes

DNA nanotubes composed of TX tiles have also been constructed and characterized [14]. TX tiles modified with thiol-containing double-stranded DNA stems projected out of the tile plane were used as the basic building blocks. TX nanotubes display a constant diameter of around 25 nm and have been observed with lengths up to 20 μm. In this section, we present high-resolution images of the constructs (TX nanotubes) and experimental evidence of their tube-like nature. DNA nanotubes represent a potential breakthrough in the self-assembly of nanometer-scale circuits for electronics layout because they can be targeted to connect at specific locations on larger-scale structures and can subsequently be metallized to form nanometer-scale metallic wires (see Section 2.6).

TX nanotube self-assemblies were formed from two DNA tile building blocks, a TAO (tile *A*) and a TAO + 2J (tile *B*) as shown in Fig. 1.8(a). The *B* tile contains two extra double-stranded DNA stems, which form junctions with the central helix of the tile such that they project out of the tile plane, with one stem protruding on each side of the tile. The *B* tiles used here are modified by the replacement of the loop on one protruding stem with a blunt end containing two thiol groups, one on a 3′ and the other on a 5′ strand terminus. Figure 1.8(b, right) shows a section of the proposed structure of the nanotubes with *B* tile layers alternating with *A* tile layers, double-stranded DNA helix axes aligned parallel with the tube axis, and thiol groups are located inside the tubes. Imaging of TX *AB* flat lattice sheets (Fig. 1.8c, left) demonstrates lattice fragments with widely varying dimensions and often with uneven edges. On the other hand, DNA nanotubes (Fig. 1.8c, right) exhibit uniform widths of around 25 nm for lengths of up to 20 μm.

Figure 1.9(a) shows a typical AFM image (tapping mode in air) of the TX nanotube. Stripes perpendicular to the long axis of the filaments are clearly visible and indicate closed ring structures in successive layers rather than a spiral structure, which would have given stripes with a noticeable diagonal slant. Figure 1.9(b) shows a high-resolution AFM image (tapping mode in buffer) of the TX nanotube in which one can discern three gaps and four tiles in some of the layers. The gaps and tiles are arrayed parallel with the axis of the flattened tube.

Burial of the sulfur moieties within the tubes makes logical sense because disulfide bridges are preferred structures formed by thiol groups under physiologic-like solution conditions such as those used here. The formation of disulfide bonds between neighboring *B* tiles would cause the lattice to curve and form tubes. The possible existence of free thiols on the outer surface of the nanotubes was probed by using two different gold reagents with reactivity toward sulfur: monomaleimido Nanogold (Nanoprobes, Yaphank, NY) and fresh colloidal gold nanoparticles. The monomaleimido Nanogold failed to react with the tube surfaces, whereas the colloidal gold displayed the interesting reactivity shown in Fig. 1.9(d and e). With very low background levels of unbound gold, the bound gold particles showed a very high probability of attachment to the ends of nanotubes and not to the outer surface anywhere else along the length of the tubes. The indication is that sulfur

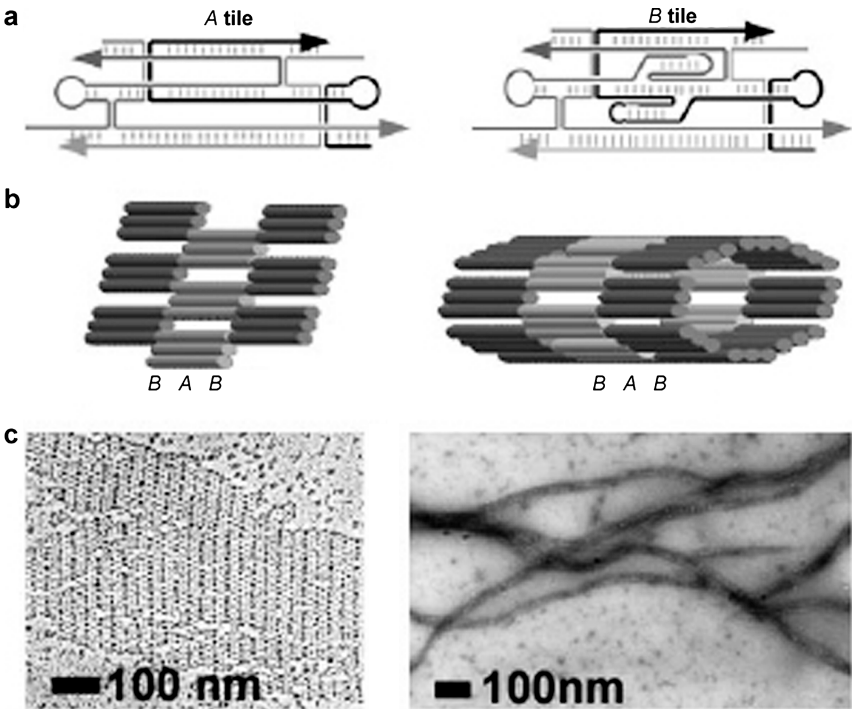

Fig. 1.8. (a) Schematic drawings showing the strand traces through the two tile types used in the constructions. Oligonucleotides are shown in different shades of gray and with arrowheads marking the 3′-ends. Short vertical hash marks indicate base pairing within double-helical regions; paired vertical lines represent crossover points. The central helices of both tile types are terminated with T_4 loops. Two extra stem–loops (2J) on the central helix of the *B* tile are designed to protrude, one into and one out of the tile plane. (b) (Left) Cartoon of a section of TAO flat lattice constructed from *A* and *B* tiles. Tubes represent double-helical regions; for simplicity, the 2J stem–loops on the *B* tiles are not shown. (Right) Cartoon model of a section of TAO nanotube shown with eight tiles per layer of tube. (c) (Left) TEM image of platinum rotary shadowed TAO lattice. The *B* tiles appear darker than the *A* tiles, having picked up more platinum on their protruding 2J stem–loops; alternating stripes of *A* and *B* tiles are clearly visible with approximately the expected distance of 28 nm. (Right) TEM image of negative-stained TAO nanotubes. (From Ref. [14].)

which is buried within the tubes is exposed to some extent at the open ends of the nanotubes and available for binding with gold. This observation, in addition to offering evidence of the location of the thiol groups, may also be exploited in future work on targeted binding or formation of electrical contacts with the ends of TX nanotubes. Final evidence of the involvement of disulfide bridges in TX nanotube formation was provided by annealing the DNA in the presence of the reducing agent dithiothreitol and observing a complete lack of tubes.

Figure 1.10 shows a series of *in situ* zoomed images showing a TX nanotube being converted to a flat lattice by the physical effect of the AFM tip. The series of

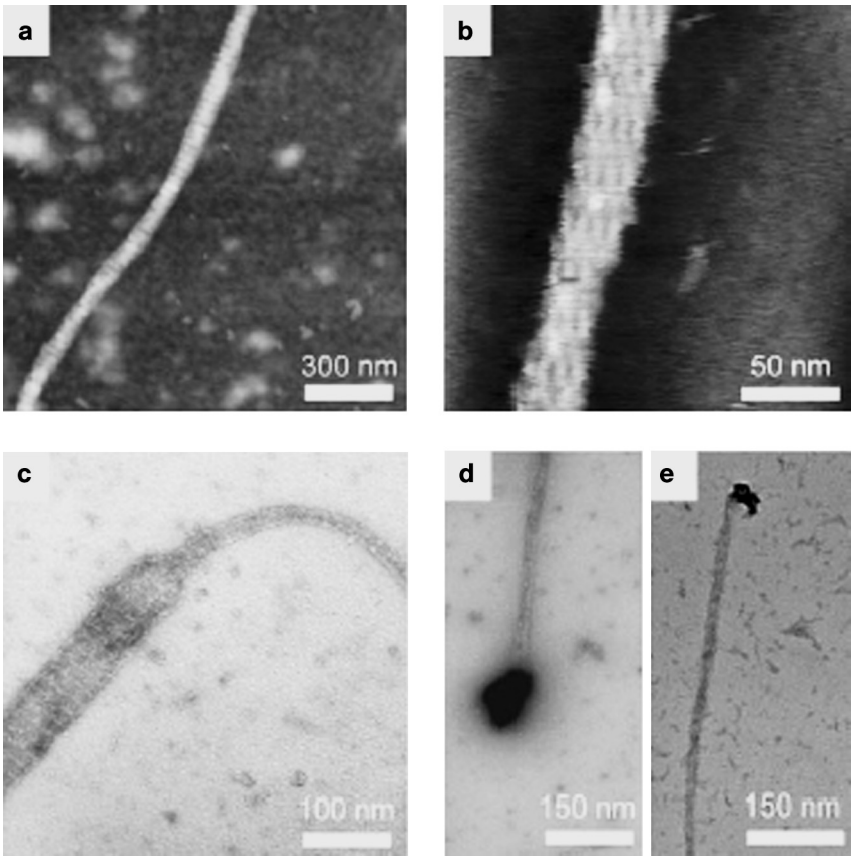

Fig. 1.9. (a) AFM image of a TAO nanotube taken by tapping mode in air. The *B* tile layers are visible as brighter stripes (because of increased height) oriented perpendicular to the long axis of the tube. (b) High-resolution image of a nanotube taken by tapping mode under buffer. Single-helix holes between adjacent tiles are visible as darker patches in several layers. (c) TEM image of a negative-stained sample, showing a section of a nanotube that appears to have split into a flat lattice. (d and e) Negative-stained TEM images of TAO nanotubes with gold nanoparticles attached to the ends, apparently by interaction with thiol sulfurs partially exposed at the tube termini. (From Ref. [14].)

images was collected by repeatedly re-imaging the same nanotube under buffer with an AFM. The high-resolution image in Fig. 1.10(d) shows the detailed nanostructure of the completely torn open DNA nanotube with alternating layers of *A* and *B* tiles clearly discernible. Whole tiles have been scratched away from the opening nanotube by the force of the AFM tip and therefore the tile layers no longer contain all of the tiles that were present in the nanotube. A few layers are seen that still contain six tiles. The combination of the high-resolution AFM images (Fig. 1.9b and 1.10d) provides supporting evidence for the model in which individual tile layers in intact nanotubes contain eight tiles.

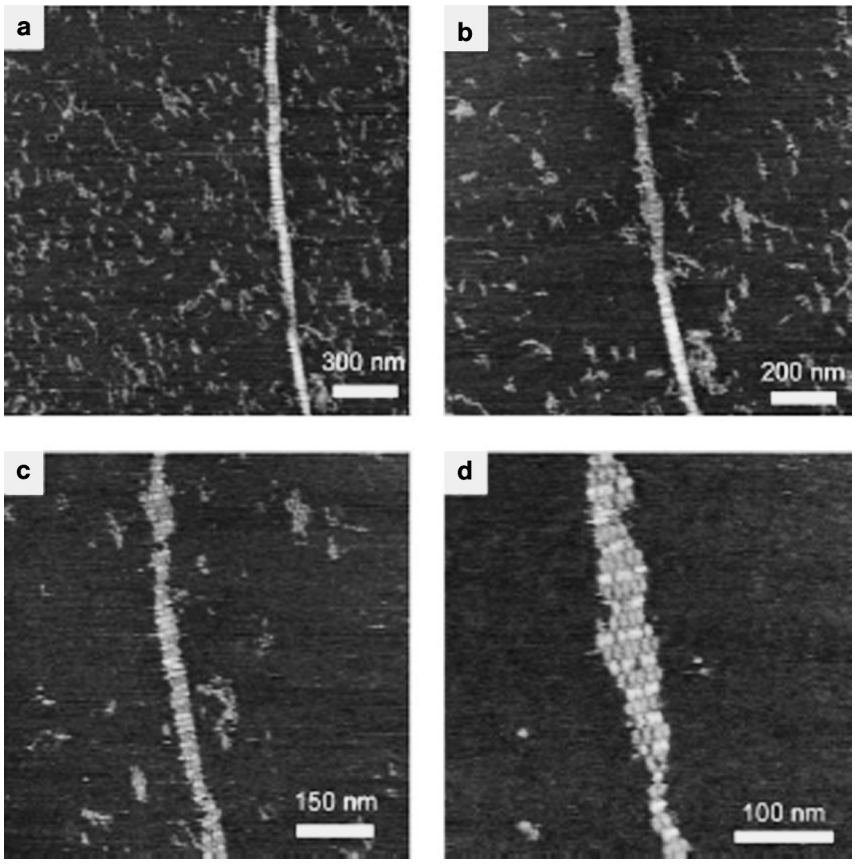

Fig. 1.10. A series of AFM images captured by repeatedly re-imaging and zooming in on the same nanotube, which appears mostly tube-like in (a), with increasing wear-and-tear through (b) and (c) until a section of unfolded tube becomes a single-layer, flat lattice (d) displaying stripes composed of lighter (higher) *B* tiles and darker (shorter) *A* tiles. (From Ref. [14].)

1.6
4 × 4 Tile Nanotubes

More complicated 1-D tube-like structure utilizing 4×4 tiles has also been reported [36]. Programmable self-assembly of this DNA nanostructure results in a uniform width nanoribbon which displays periodic square cavities. The 4×4 DNA tile (Fig. 1.11a) contains four four-armed DNA branched junctions pointing in four directions – north, south, east and west in the tile plane. It is composed of nine strands, with one of the strands participating in every junction. Bulged T_4 loops are placed at each of the four corners inside the tile core in order to decrease the probability of stacking interactions between adjacent four-arm junctions and

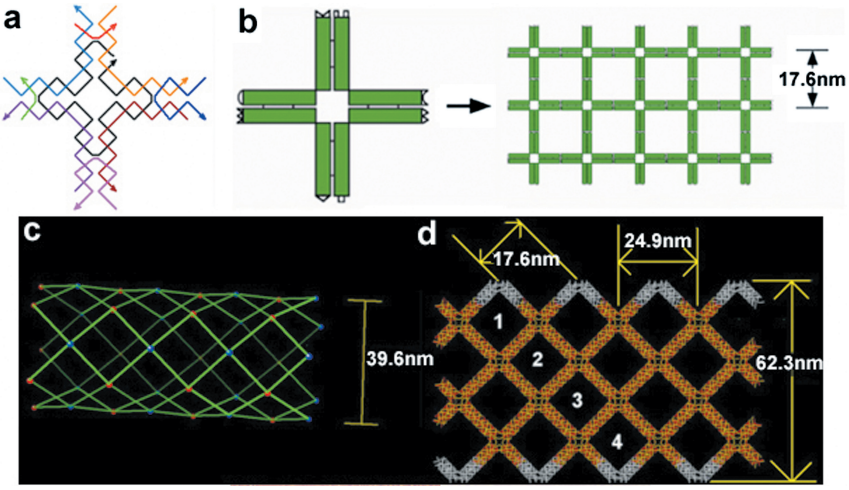

Fig. 1.11. Self-assembly of DNA nanoribbons using the 4 × 4 DNA tile. (a) The 4 × 4 tile strand structure. The tile contains nine oligonucleotides, shown as simplified backbone traces in different colors. Each four-arm junction is oriented in four directions. The black strand participates in all four junctions and contains T_4 loops connecting adjacent junctions. (b) Left: double-helical domains are illustrated as rectangles and paired rectangles represent four-arm junctions. Watson–Crick complementary sticky ends are shown as matching geometric shapes. Right: designed structure of the self-assembled lattice. There are four full helical turns between tile centers so the tiles will be oriented in the same direction in the lattice. (c) Schematic model of the proposed 4 × 4 nanotube. (d) Overhead view of a tube squashed onto the mica substrate and forming a ribbon with four diagonal square cavities with a width of around 62.3 nm. Note the saw-tooth edge formed by folding one row of 4 × 4 tiles along a diagonal running through their most flexible region, the T_4 loops between adjacent arms. The jagged edges along with the 45° diagonal containing four cavities are typically observed in high-resolution AFM images of the ribbons. (From Ref. [36].)

allow the arms to point to four different directions. Characterization of structure formation by nondenaturing gel electrophoresis and thermal transition analysis (see Fig. 1.13 below) shows that the 4 × 4 tile structure is stable and well behaved.

Constructions following the design shown in Fig. 1.11(b) produce a high preponderance of uniform width ribbon structures. In this design the distance between adjacent tiles is an even number of helical half-turns (four full turns) so that the identical face of each tile points toward the same lattice face. Figure 1.12 shows four AFM images of the nanoribbons with lengths of up to around 20 μm and a typical uniform width of around 60 nm. The regularity of the periodic cavities is striking, as well as the observation that some of the nanoribbons revealed a single-layer, flat grid lattice unrolled at the open end of the ribbon (see Fig. 1.12d). This observation strongly suggests that the ribbon structure results from tube-like structures which flatten when the sample is deposited on mica. The AFM image height profile clearly shows that the nanoribbon structure has two layers compared to the flat lattice. Also, the edges of the ribbon appear slightly higher, about 0.12 nm,

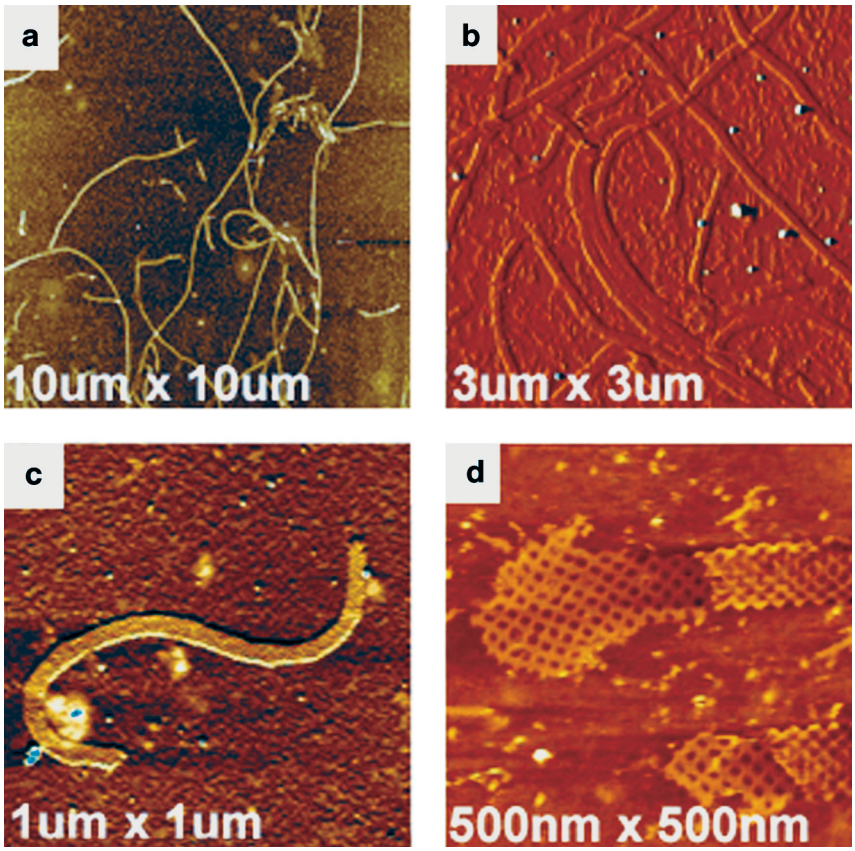

Fig. 1.12. AFM images of 4 × 4 nanoribbons at various scan sizes. (From Ref. [36].)

than the middle, indicating a finite radius of curvature for the squashed tube structure. The formation of tube-like lattices could be due to the fact that each component tile is oriented in the same direction in the designed lattice planes, and therefore any incidental curvature resident in each tile could accumulate and cause circularization of the lattice. This hypothesis is supported by the AFM analysis and by subsequent experiments showing that corrugation schemes where tiles are flipped in the lattice plane to compensate for tile curvature form large flat lattice sheets.

1.7 6HB Tile Nanotubes

Very recently, a new strategy for the creation of hollow DNA nanotubes was described which made use of tiles that are intrinsically 3-D and formed from a rigid

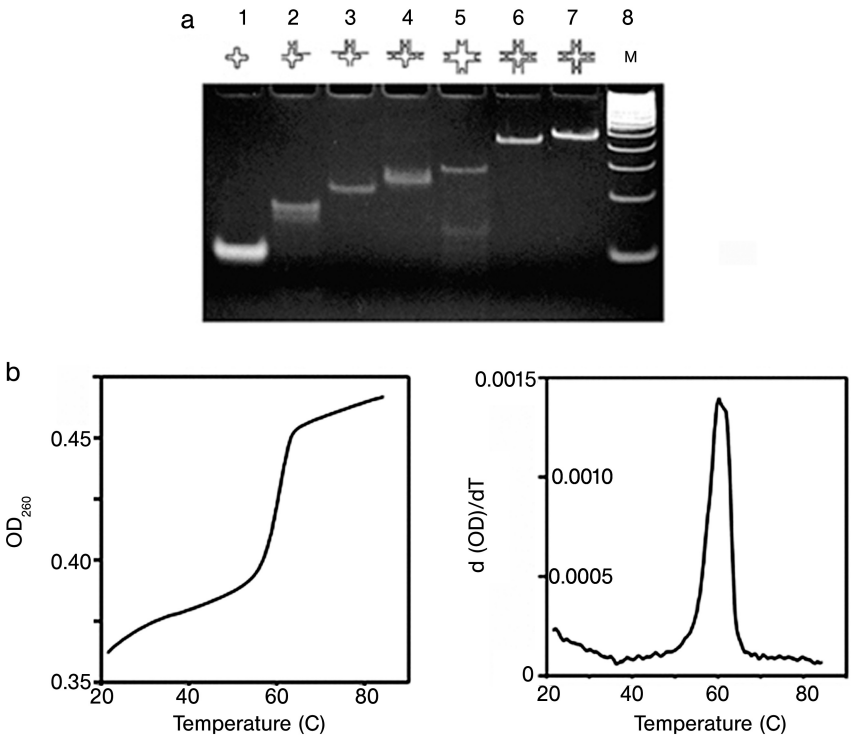

Fig. 1.13. Characterization of the 4 × 4 tile structure using nondenaturing electrophoresis and thermal transition experiments. (a) An 8% polyacrylamide gel (ethidium bromide stained) showing association complexes between various equimolar combinations of the 4 × 4 DNA complex component strands. Equimolar mixtures at 1 μM concentration per included strand were annealed and run on the gel at room temperature. Strands included in the annealings are indicated in the drawing above each lane. Lane 8 contains a 50-bp DNA ladder size marker. The 4 × 4 complex runs as a single band on nondenaturing gels, without any higher-molecular-weight byproducts (from unexpected base pairings between two or more complexes) or lower-molecular-weight byproducts (from dissociated complex), indicating the 4 × 4 tile complex is a stable structure in the buffer used. (b) Thermal transition profile. The left panel shows the relative change in optical density at 260 nm as a function of temperature. The right panel shows the first derivative of the 4 × 4 complex melting data. The results show that the 4 × 4 complex melts cooperatively, as a single transition, with $T_m \sim 60\,^{\circ}C$. (From Ref. [36].)

cluster of double-helical domains with a single-helix width pore running down through its entire length [37]. The 6HB (shown schematically in Fig. 1.14) contained six double helices with each pair of neighboring domains linked by strand exchange at each of two crossover points. With complementary pairs of sticky ends appended to each end of the helices, the tiles were induced to assemble into long 1-D arrays with lengths up to around 15 μm. These are the first described DNA nanotubes with perfectly designed widths and tube layers made up of single tiles.

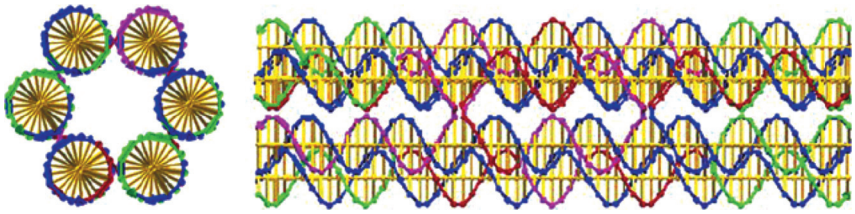

Fig. 1.14. Cross-sectional and transverse views of the 6HB tile model. The cross-sectional view emphasizes the cylindrical hole through the center of the tile (From Ref. [37].)

1.8 Applications

Self-assembled 1-D nanotubes made from artificially designed tiles show great promise for applications that range from fabrication of nanoelectronic devices to biological studies. Electrical transport in bare DNA molecules has been recognized as an interesting research field for last few decades. Although some of the conductivity experiments of DNA molecules had been shown superconducting [39] or semiconducting [40] properties, DNA molecules mostly show insulating characteristic [41]. The DNA molecule's poor conductivity prevents its direct use in electronic nanodevices. Thus, properly designed DNA lattices can serve as a precisely controllable and programmable scaffold for organizing functionalized nanomaterials in the design and construction of functionalized electronic nanodevices. Nanometer-scale fabrication with reliable DNA-templated metallic nanowires is an example demonstration of DNA's scaffolding capability. Several varieties of DNA tile nanotubes have been shown to be useful templates for the specific chemical deposition of metal for nanowire formation.

Until now, mostly natural λ DNA molecules have been used as a template for fabricating various metallic nanowires such as silver [42], gold [43], palladium [44, 45], platinum [46] and copper [47]. More complex and uniform width 1-D nanotubes can also serve as templates for highly conductive metallic nanowires. One example is shown in Fig. 1.15. Here, 4×4 nanoribbons have been metallized with silver using a novel electroless chemical deposition technique [36] and demonstrated electrical measurements through silver nanowires. The resulting nanowires have been characterized by scanning electron microscopy (SEM) and AFM. The metallized nanoribbons have heights of 35 ± 2 nm, widths of 43 ± 2 nm and lengths of up to about 5 μm. The current–voltage curve of the metallic silver 4×4 nanoribbon shows linear behavior and the resistance of this sample is around 200 Ω as measured between the two central contacts at a bias voltage of 0.1 V (Fig. 1.15c). This number corresponds to a bulk resistivity of 2.4×10^{-6} Ωm. This nanowire is easily reproducible and has markedly higher conductivity than previously reported double-helix DNA-templated silver nanowires [42]. Other potential uses of DNA nanotubes are inspired by analogy with the roles of nanotubes and nanowires in living cells, e.g. as structural supports for the cytoskeleton, as tracks for

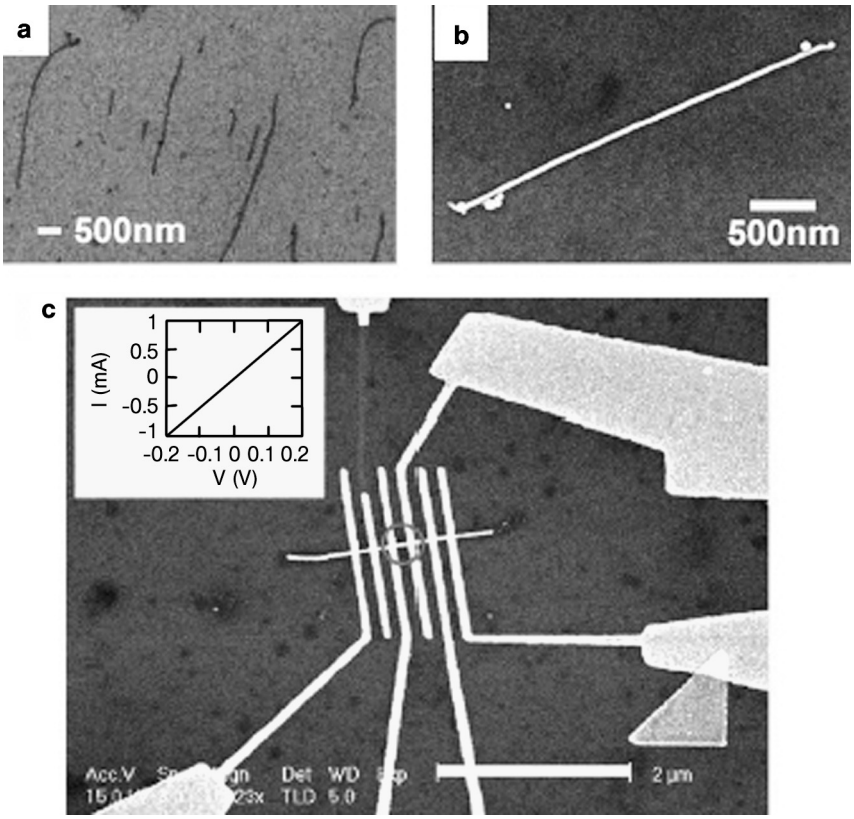

Fig. 1.15. Metallization and a conductivity measurement of metallized 4 × 4 nanoribbons. (a) SEM image of nonmetallized 4 × 4 nanoribbons. (b) SEM image of silver-seeded silver nanoribbon. The change in the signal contrast between (a) and (b) is apparent. (c) SEM image of the actual device (scale bar: 2 µm). (Inset) Current–voltage curve of the metallic silver 4 × 4 nanoribbon. (From Ref. [36].)

the transport of microscopic cargo and as moving parts for cellular motility. DNA nanotubes may eventually be engineered to mimic all these functions.

1.9 Summary and Perspectives

DNA-based nanotechnology is currently being developed as a general assembly method for nanopatterned materials that may find use in electronics, sensors, medicine and many other fields. In this chapter, we have described a novel assembly of 1-D nanotubes made from artificially designed tiles, DX, TX, 4 × 4 and 6BH branched junction tiles. Nanotubes, consisting of DAE-E tiles, range from 7 to

20 nm in diameter, grow as long as 50 μm with a persistence length of around 4 μm, and can be programmed to display a variety of patterns. DAE-O DX tiles can form sheets or ribbons with periodic banding controlled by salt concentration. TX nanotubes display a constant diameter of around 25 nm and have been observed with lengths up to 20 μm. Tube formation is controlled by disulfide bonds between tiles augmented with thiol moieties. The 4 × 4 DNA nanoribbon contains four four-armed DNA branched junctions pointing in four directions. The formation of tube-like lattices is due to the fact that each component tile is oriented in the same direction in the designed lattice plane, and therefore any incidental curvature resident in each tile can accumulate and cause circularization of the lattice. The 1-D arrays of 6HB tiles form DNA nanotubes with one tile per tube layer and represent the smallest possible hollow DNA nanotube. Nanotubes formed from DNA tile lattices have been used as metallization templates for the formation of conductive nanowires. Utilizing DNA molecules as scaffolds for making functionalized nanowires offers certain advantages such as site-specific alignment and massive, parallel self-assembly for future electronic nanodevices. It has also been pointed out that DNA nanotubes, by analogy with cellular microtubules, might be useful as tracks along which artificial bionanomachines might transport molecular cargo [10, 12].

References

1 Seeman, N. C., DNA in a material world, *Nature* **2003**, *421*, 427–431.

2 Xu, J., LaBean, T. H., Craig, S. L., DNA-based structures and their applications in nanotechnology. In *Supramolecular Polymers 2*, Ciferri, A. (Ed.), Taylor & Francis, Boca Raton, FL, **2005**, pp. 445–480.

3 Seeman, N. C., Nucleic acid nanostructures and topology, *Angew. Chem. Int. Ed.* **1998**, *37*, 3220–3238.

4 Seeman, N. C., Nucleic-acid junctions and lattices, *J. Theor. Biol.* **1982**, *99*, 237–247.

5 Seeman, N. C., *De novo* design of sequences for nucleic acid structural engineering, *J. Biomol. Struct. Dyn.* **1990**, *8*, 573–581.

6 Seeman, N. C., Wang, H., Yang, X., Liu, F., Mao, C., Sun, W., Wenzler, L., Shen, Z., Sha, R., Yan, H., Wong, M. H., Sa-Ardyen, P., Liu, B., Qiu, H., Li, X., Qi, J., Du, S. M., Zhang, Y., Mueller, J. E., Fu, T., Wang, Y., Chen, J., New motifs in DNA nanotechnology, *Nanotechnology* **1998**, *9*, 257–273.

7 Liu, F., Sha, R., Seeman, N. C., Modifying the surface features of two-dimensional DNA crystals, *J. Am. Chem. Soc.* **1999**, *121*, 917–922.

8 Winfree, E., Liu, F., Wenzler, L. A., Seeman, N. C., Design and self-assembly of two-dimensional DNA crystals, *Nature* **1998**, *394*, 539–544.

9 Mao, C., Sun, W., Seeman, N. C., Designed two-dimensional DNA Holliday junction arrays visualized by atomic force microscopy, *J. Am. Chem. Soc.* **1999**, *121*, 5437–5442.

10 Rothemund, P., Ekani-Nkodo, A., Papadakis, N., Kumar, A., Fygenson, D. K., Winfree, E., Design and characterization of programmable DNA nanotubes, *J. Am. Chem. Soc.* **2004**, *126*, 16344–16352.

11 Ekani-Nkodo, A., Kumar, A., Fygenson, D. K., Joining and scission in the self-assembly of nanotubes from DNA tiles, *Phys. Rev. Lett.* **2004**, *93*, 2683011–2683014.

12 Mitchell, J. C., Robin-Harris, J., Malo, J., Bath, J., Turberfield, A. J., Self-assembly of chiral DNA nanotubes, *J. Am. Chem. Soc.* **2004**, *126*, 16342–16343.

13 Li, H., Park, S. H., Reif, J. H., LaBean, T. H., Yan, H., DNA-templated self-assembly of protein and nanoparticle linear arrays, *J. Am. Chem. Soc.* **2004**, *126*, 418–419.

14 Liu, D., Park, S. H., Reif, J. H., LaBean, T. H., DNA nanotubes self-assembled from triple-crossover tiles as templates for conductive nanowires, *Proc. Natl Acad. Sci. USA* **2004**, *101*, 717–722.

15 Zhang, Y., Seeman, N. C., The construction of a DNA truncated octahedron, *J. Am. Chem. Soc.* **1994**, *116*, 1661–1669.

16 Shih, W. M., Quispe, J. D., Joyce, G. F., A 1.7-kilobase single-stranded DNA that folds into a nanoscale octahedron, *Nature* **2004**, *427*, 618–621.

17 Mao, C., Sun, W., Shen, Z., Seeman, N. C., A DNA nanomechanical device based on the B–Z transition, *Nature* **1999**, *397*, 144–146.

18 Yurke, B., Turberfield, A. J., Mills, A. P., Simmel, F., Neumann, J. L., A DNA-fueled molecular machine made of DNA, *Nature* **2000**, *406*, 605–608.

19 Yan, H., Zhang, X., Shen, Z., Seeman, N. C., A robust DNA mechanical device controlled by hybridization topology, *Nature* **2002**, *415*, 62–65.

20 Turberfield, A. J., Mitchell, J. C., DNA fuel for free-running nanomachines, *Phys. Rev. Lett.* **2003**, *90*, 1181021–1181024.

21 Shen, Z., Yan, H., Wang, T., Seeman, N. C., Paranemic crossover DNA: a generalized Holliday structure with applications in nanotechnology, *J. Am. Chem. Soc.* **2004**, *126*, 1666–1674.

22 Peng, L., Park, S. H., Reif, J. H., Yan, H., A two-state DNA lattice switched by DNA nanoactuator, *Angew. Chem. Int. Ed.* **2003**, *42*, 4342–4346.

23 Yin, P., Yan, H., Daniell, X. G., Turberfield, A. J., Reif, J. H., A unidirectional DNA walker that moves autonomously along a track, *Angew. Chem. Int. Ed.* **2004**, *43*, 4906–4911.

24 Adleman, L., Molecular computation of solutions to combinatorial problems, *Science* **1994**, *266*, 1021–1024.

25 Winfree, E., Algorithmic self-assembly of DNA: theoretical motivations and 2D assembly experiments, *J. Biomol. Struct. Dyn.* **2000**, *11*, 263–270.

26 Mao, C., LaBean, T. H., Reif, J. H., Seeman, N. C., Logical computation using algorithmic self-assembly of DNA triple crossover molecules, *Nature* **2000**, *407*, 493–496.

27 Benenson, Y., Paz-Elizur, T., Adar, R., Keinan, E., Livneh, Z., Shapiro, E., Programmable and autonomous computing machine made of biomolecules, *Nature* **2001**, *414*, 430–434.

28 Ravinderjit, B., Chelyapov, N., Johnson, C., Rothemund, P., Adleman, L., Solution of a 20-variable 3-SAT problem on a DNA computer, *Science* **2002**, *296*, 499–502.

29 Dwyer, C., Poulton, J., Taylor, R., Vicci, L., DNA self-assembled parallel computer architectures, *Nanotechnology* **2004**, *15*, 1688–1694.

30 Rothemund, P., Papadakis, N., Winfree, E., Algorithmic self-assembly of DNA Sierpinski triangles, *PLOS Biol.* **2004**, *2*, 2041–2053.

31 Niemeyer, C. M., Burger, W., Peplies, J., Covalvent DNA–streptavidin conjugates as building blocks for novel biometallic nanostructures, *Angew. Chem. Int. Ed.* **1998**, *37*, 2265–2268.

32 Storhoff, J. J., Mirkin, C. A., Programmed materials synthesis with DNA, *Chem. Rev.* **1999**, *99*, 1849–1862.

33 Baker, S. E., Cai, W., Lasseter, T. L., Weidkamp, K. P., Hamers, R. J., Covalently bonded adducts of deoxyribonucleic acid oligonucleotides with single-wall carbon nanotubes, *Nano Lett.* **2002**, *2*, 1413–1417.

34 Fu, T., Seeman, N. C., DNA double-crossover molecules, *Biochemistry* **1993**, *32*, 3211–3220.

35 LaBean, T. H., Yan, H., Kopatsch, J., Liu, F., Winfree, E., Reif, J. H., Seeman, N. C., Construction, analysis,

ligation, and self-assembly of DNA triple crossover complexes, *J. Am. Chem. Soc.* **2000**, *122*, 1848–1860.

36 Yan, H., Park, S. H., Finkelstein, G., Reif, J. H., LaBean, T. H., DNA-templated self-assembly of protein arrays and highly conductive nanowires, *Science* **2003**, *301*, 1882–1884.

37 Mathieu, F., Liao, S., Kopatsch, J., Wang, T., Mao, C., Seeman, N. C., Six-helix bundles designed from DNA, *Nano Lett.* **2005**, *5*, 661–665.

38 Dresselhaus, M. S., Dresselhaus, G., Eklund, P. C., *Science of Fullerenes and Carbon Nanotubes*, Academic Press, New York, **1996**.

39 Kasumov, A., Kociak, M., Gueron, S., Reulet, B., Volkov, V. T., Klinov, D. V., Bouchiat, H., Proximity-induced superconductivity in DNA, *Science* **2001**, *291*, 280–282.

40 Porath, D., Bezryadin, A., de Vries, S., Dekker, C., Direct measurement of electrical transport through DNA molecules, *Nature* **2000**, *403*, 635–638.

41 Storm, A., van Noort, J., de Vries, S., Dekker, C., Insulating behavior for DNA molecules between nanoelectrodes at the 100 nm length scale, *Appl. Phys. Lett.* **2001**, *79*, 3881–3883.

42 Braun, E., Eichen, Y., Sivan, U., Ben-Yoseph, G., DNA-templated assembly and electrode attachment of a conducting silver wire, *Nature* **1998**, *391*, 775–778.

43 Patolsky, F., Weizmann, Y., Lioubashevski, O., Willner, I., Au-nanoparticle nanowires Based on DNA and polylysine templates, *Angew. Chem. Int. Ed.* **2002**, *41*, 2323–2327.

44 Richter, J., Mertig, M., Pompe, W., Monch, I., Schackert, H., Construction of highly conductive nanowires on a DNA template, *Appl. Phys. Lett.* **2001**, *78*, 536–538.

45 Deng, Z., Mao, C., DNA-templated fabrication of 1D parallel and 2D crossed metallic nanowire arrays, *Nano Lett.* **2003**, *3*, 1545–1548.

46 Ford, W. E., Harnack, O., Yasuda, A., Wessels, J., Platinated DNA as precursors to templated chains of metal nanoparticles, *Adv. Mater.* **2001**, *13*, 1793–1797.

47 Monson, C. F., Woolley, A. T., DNA-templated construction of copper nanowires, *Nano Lett.* **2003**, *3*, 359–363.